



HAL
open science

Observations of the low-lying $\Omega = 1/2$ states of nickel deuteride, NiD

Amanda J. Ross, Patrick Crozet, Allan Adam, Dennis W. Tokaryk

► **To cite this version:**

Amanda J. Ross, Patrick Crozet, Allan Adam, Dennis W. Tokaryk. Observations of the low-lying $\Omega = 1/2$ states of nickel deuteride, NiD. *Journal of Molecular Spectroscopy*, 2019, 362, pp.45-55. 10.1016/j.jms.2019.06.003 . hal-02158677

HAL Id: hal-02158677

<https://hal.science/hal-02158677>

Submitted on 25 Oct 2019

HAL is a multi-disciplinary open access archive for the deposit and dissemination of scientific research documents, whether they are published or not. The documents may come from teaching and research institutions in France or abroad, or from public or private research centers.

L'archive ouverte pluridisciplinaire **HAL**, est destinée au dépôt et à la diffusion de documents scientifiques de niveau recherche, publiés ou non, émanant des établissements d'enseignement et de recherche français ou étrangers, des laboratoires publics ou privés.

Observations of the low-lying $\Omega=1/2$ states of nickel deuteride, NiD

Amanda J. Ross¹, Patrick Crozet¹, Allan G. Adam³, Dennis W. Tokaryk²

1) Institut Lumière Matière, Université Lyon 1 and CNRS, Université de Lyon, France

2) Physics Department, University of New Brunswick, Fredericton, New Brunswick, Canada E3B 5A3

3) Chemistry Department, University of New Brunswick, Fredericton, New Brunswick, Canada E3B 5A3

Keywords

NiH, NiD, Fourier transform laser-induced fluorescence, transition metal hydride

Highlights

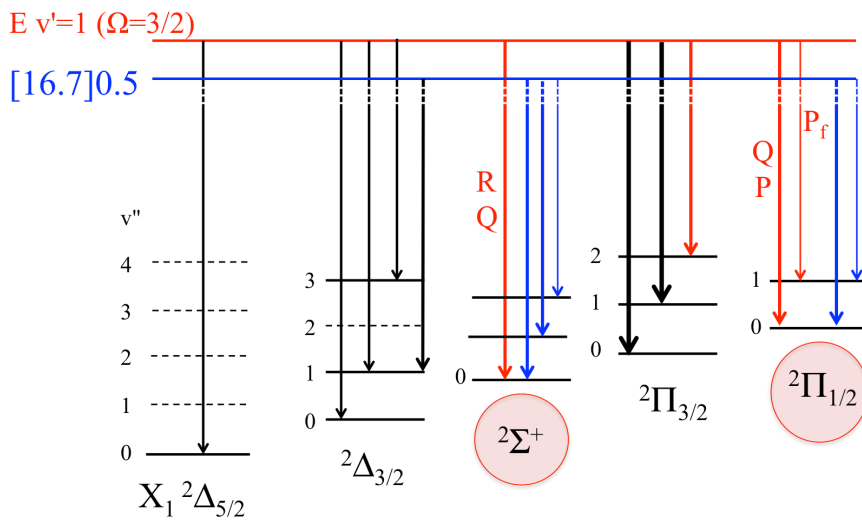
- Vibrational levels of the low-lying $^2\Sigma^+$ and $^2\Pi_{1/2}$ states have been located in ^{58}NiD
- Analysis validate predictions from a multi-isotope supermultiplet fit
- A new electronic $\Omega' = 0.5$ state has been identified, with $T'_v \sim 16724.5 \text{ cm}^{-1}$ above the first rotational level of the ground state.

Abstract

While the spectrum of NiH has been extensively studied, only the $\Omega=3/2$ and $5/2$ components of the strongly interacting $^2\Delta$, $^2\Pi$ and $^2\Sigma^+$ molecular states arising from the $3d^9$ ground-state configuration of Ni^+ have been reported for the deuterated form, NiD. We report on laser excitation and resolved fluorescence experiments that definitively locate rotational levels of $v=0-2$ in the $^2\Sigma^+$ state, and of $v=0$ and $v=1$ in the low-lying $^2\Pi_{1/2}$ state of ^{58}NiD .

Graphical Abstract

Resolved fluorescence in NiD



Introduction

This investigation of dispersed fluorescence in NiD was motivated by attempts to use isotopic substitution to improve a 'global' description of the three low-lying electronic states ($^2\Delta$, $^2\Pi$, $^2\Sigma^+$) of Ni $^{1,2}\text{H}$, either through 'supermultiplet' models [1], or potential energy curve fits [2]. The three lowest-lying electronic states of NiH show strong effects of spin-orbit interactions, resulting in irregular vibrational spacings in all but the $^2\Delta_{5/2}$ ground state. The upper states accessible to visible laser excitation are associated with f-d excitation on Ni atoms, the strongest transitions being to upper states with significant $^2\Delta_{5/2}$ or $^2\Phi_{7/2}$ character.

Resolved laser-induced fluorescence from $\Omega' = 3/2, 5/2$ and $7/2$ excited states [3] has recently located vibrational levels of $^2\Delta_{5/2}$, $^2\Delta_{3/2}$ and $^2\Pi_{3/2}$ in NiD, (corresponding quite closely to the three low-lying electronic states of NiCN reported by Kingston, Merer and Varberg [4]) but provided no information about the $\Omega'' = 1/2$ states. The low-lying $^2\Pi_{1/2}$ and $^2\Sigma^+$ states of NiH were observed via collisional energy transfer between close-lying excited states, in particular to an $\Omega'=1/2$ upper state [5], but there was no evidence of an equivalent process in the NiD spectra discussed in ref. [3].

Survey spectra.

The analysis of ref. [3] was severely hampered by lack of information on the two $\Omega=1/2$ components of the Ni $^+(3d^9)$ -D $^-$ supermultiplet, so the objective here was to determine as many rovibrational term values as possible for the low-lying $^2\Sigma^+$ and $^2\Pi_{1/2}$ states. The hybrid Hund's case (a) -Hund's case (b) Hamiltonian proposed by Abbasi in [3] predicted their first rotational levels ($v=0$) to be respectively ~ 2073 and 3507 cm^{-1} above the lowest level of the electronic ground state, but the predictive powers of this model were so far untested. We reasoned that whilst $\Delta\Omega = \Delta\Lambda$ (and particularly $\Delta\Lambda=0$) transitions are the strongest in the visible systems of NiH and NiD, some $\Delta\Omega = \pm 1$ systems are observed. A (weak) $^2\Pi_{3/2} \leftarrow ^2\Delta_{5/2}$ pump transition could conceivably yield (even weaker) $^2\Pi_{3/2} \rightarrow ^2\Sigma^+$ fluorescence. We surveyed the excitation spectrum of NiD in an experiment similar to those performed by Guo *et al.* on NiH [6]. NiD was produced in the collision-free environment of a molecular-jet laser-ablation source at University of New Brunswick, using CD $_4$ as a precursor. A pulsed dye laser (YAG-pumped Hyperdye HD-500, repetition rate 10 Hz, resolution approximately 0.1 cm^{-1}) was scanned from 16000 to 18580 cm^{-1} , detecting through a 0.25 m monochromator (zero order) and using $\lambda > 610$ or 640 nm filters to reduce laser scatter, since the signals of primary interest – to excited electronic states – were expected to occur more than 1500 cm^{-1} below the laser line. Dispersed fluorescence from each

resonance was then recorded at low resolution with a 0.5 m monochromator and red-sensitive Hamamatsu R-928 photomultiplier tube, to see whether there were any features likely to correspond to emission to $\Omega'' = \frac{1}{2}$ states. The only excitations to show any promise were those exciting the first rotational levels of E [17.5]1.5 ($v=1$), using $[T_v'$ in $1000 \text{ cm}^{-1}] \Omega$ notation. This upper state had already been identified in ref. [3] from collisionally-induced emission to ${}^2\Pi_{3/2}$, but no $E \rightarrow {}^2\Sigma^+$ transitions had been found. Direct excitation of E[17.5]1.5 (and D[17.2]1.5) had also been attempted, but gave emission signals too weak to record in Fourier transform resolved fluorescence. In the collision-free ablation source environment, with all population concentrated in the lowest rotational levels, the strong feature around 15450 cm^{-1} (see Figure 1) was readily assigned as $E \rightarrow {}^2\Sigma^+$ ($v=0$) emission, since it falls, as predicted, in the gap between transitions to $v=1$ of the ground state and to $v=0$ of the ${}^2\Pi_{3/2}$ state. The peaks around 14100 cm^{-1} were not immediately assignable; on energetic grounds, they could plausibly come from transitions either to $v=1$ of ${}^2\Sigma^+$, or to $v=0$ of the ${}^2\Pi_{1/2}$ state.

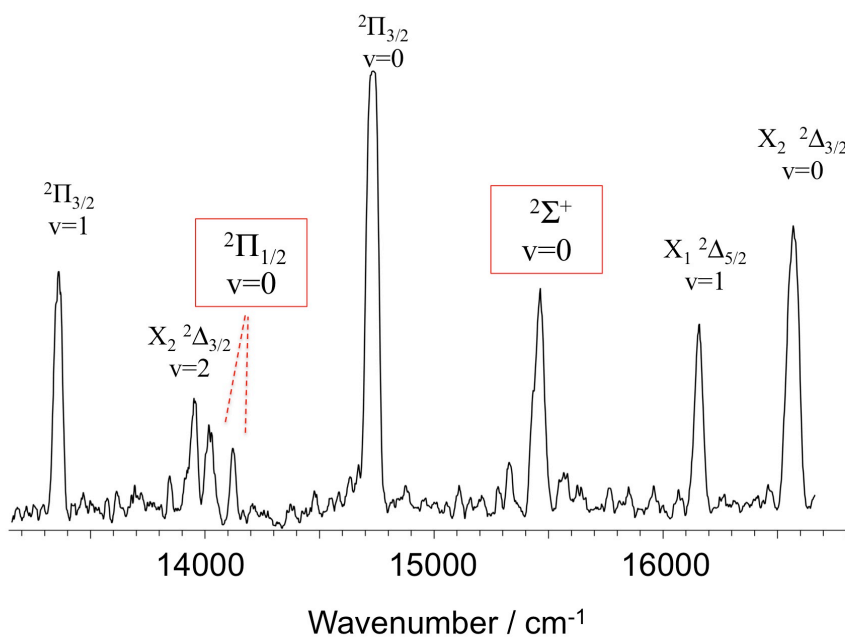


Fig 1. (in colour online) Low-resolution dispersed fluorescence in NiD. The laser (17507.5 cm^{-1}) excited $P(2.5) E [17.5]1.5 \leftarrow X_1 {}^2\Delta_{5/2} (1-0)$. Boxes indicate the transitions of particular interest, to previously unobserved low-lying electronic states.

Dispersed fluorescence at higher resolution

The low-resolution dispersed fluorescence spectrum gave convincing evidence of transitions at least to $v=0$ of the ${}^2\Sigma^+$ state, but with insufficient precision to test or refine existing predictions. Given earlier failure to record laser-induced fluorescence following $E \leftarrow X$ excitation with the Lyon experiment, we attempted a two-laser experiment with the ablation source, counter-

propagating output from two pulsed dye lasers (rhodamine 6G to pump $E \leftarrow X$, and DCM to dump $E \rightarrow {}^2\Sigma^+$), and looking for depletion while monitoring fluorescence with the monochromator set 2800 cm^{-1} below the laser, i.e. at the strongest band in Figure 1. This was unsuccessful, because issues with electrical noise from the lasers made it impossible to find the signals needed to adjust timing of the laser pulses. Not having cw laser resources to perform a high-resolution depletion experiment with the collision-free source at UNB, we were forced to revert to the Lyon experiment to take this further, using the sputter source described in detail in ref.[7].

We needed an approximately three-fold increase in signal/noise ratio compared with spectra reported in [3], to produce workable interferograms. To achieve this, we worked with a higher enrichment (15%) of D_2 in argon ("Mélange Crystal" from Air Liquide). We also passed the laser beam as close as possible to the annular anode, where the concentration of NiD radicals is highest. There are disadvantages to doing this: background scatter is higher, collisions transfer excited state population to other electronic states very efficiently, and the molecular fluorescence at the longer-wavelength end of the spectrum is dwarfed by argon atomic emission (see Figure 2). Even with maximum amplification from the Si-avalanche detector and (Bomem DA3) interferometer's amplifier, the maximum signal at zero-path difference rarely exceeded 3% of the analog-digital converter's $\pm 10 \text{ V}$ full-scale input. Nevertheless, by averaging typically 50 scans (recording time roughly 1 hour) at close to Doppler resolution (instrumental resolution 0.04 cm^{-1} in most cases), we could identify direct fluorescence to $v=0$ levels of the ${}^2\Sigma^+$ quite easily – and made use of the argon lines to verify wavenumber calibration from the Fourier transform spectrometer.

Figure 2 illustrates fluorescence from $v'=1$ of the E state, with the ring dye laser tuned to excite just one of the parity components ($J'=1.5, f$) accessed with the pulsed laser in Figure 1. We recorded 16 spectra following excitation of a selection of rotational levels ($1.5 \leq J_{e,f} \leq 11.5$) of E [17.5]1.5 ($v=1$). The R and Q branches were relatively strong in transitions to $v=0$ of ${}^2\Sigma^+$; the P branches were stronger in transitions to $v=0$ ${}^2\Pi_{1/2}$, with the R branches dying out quickly with increasing J (see Table 1). The transitions to $v=0$ of ${}^2\Pi_{1/2}$ were convincingly identified and assigned by subtracting spectra of different upper-state parity at given J , as illustrated in Figure 3. This approach removed all the 'common to both' collisionally induced emission, and greatly reduced the atomic argon lines, so that some very weak features $12600\text{-}12650 \text{ cm}^{-1}$ were tentatively assigned (and later confirmed) as P_f transitions to ${}^2\Pi_{1/2}$, $v=1$, with no hint of any branch to levels of the other parity.

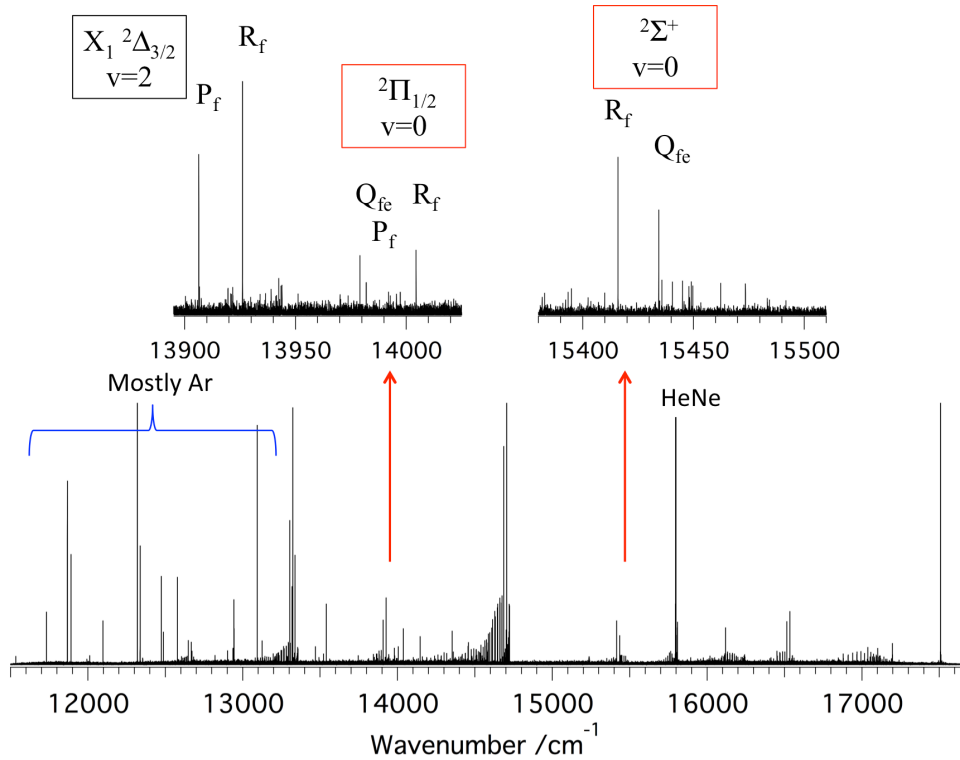


Figure 2. (in colour online) Fourier-transform record (0.04 cm^{-1} resolution) of fluorescence from $E [17.5] \Omega = 1.5, \nu = 1, J = 1.5f$ in ^{58}NiD , using a sputter source to produce NiD . The vertical arrows show enlargements of the regions with transitions to $\nu = 0$ of $^2\Pi_{1/2}$ and $^2\Sigma^+$ states, where direct fluorescence from $J' = 1.5f$ can be distinguished from a baseline of many collisionally induced, (rotationally unselective) transitions.

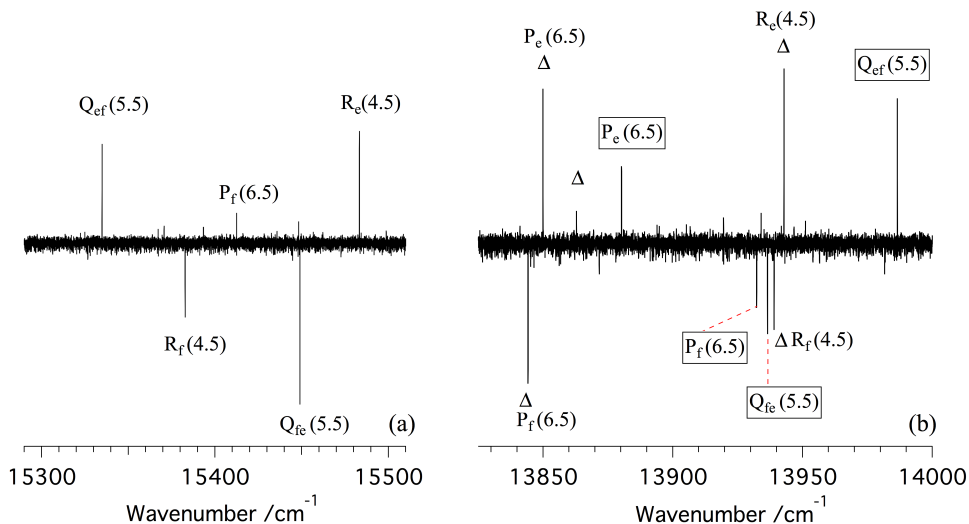


Figure 3 (in colour online). Taking the difference between spectra differing only in upper state parity for the pump transition ($E, \nu = 1, J = 5.5e$ and $5.5f$ in this example) makes direct fluorescence easier to distinguish from collisionally-induced relaxation. View (a) shows transitions to $^2\Sigma^+ \nu = 0$, and view (b) illustrates weaker transitions to $\nu = 0$ of $^2\Pi_{1/2}$, surrounded by P and R transitions to $\nu = 2$ $^2\Delta_{3/2}$ (denoted by Δ symbols), with much smaller parity splittings in the lower state.

The strongest features in the lower part of Figure 2 are rotationally relaxed E[17.5]1.5 \rightarrow $^2\Pi_{3/2}(1-0)$ and (1-1) bands. The (1-2) band of this system, near 12000 cm^{-1} , is hardly perceptible in Fig 2, but it locates previously unobserved rotational levels of $^2\Pi_{3/2}$, some 5500 cm^{-1} above the electronic ground state. Other bands have been identified as E[17.5]1.5 \rightarrow $^2\Delta_{3/2}$ ($v''=0,1,3$) and E[17.5]1.5 \rightarrow $^2\Delta_{5/2}(1-0)$. These bring no new information on the energy level patterns in NiD, but establish upper state energies with respect to the known low-lying $^2\Delta_{\Omega}$ states. Table 1 lists assigned transitions from the E[17.5]1.5 state. These transitions were included in the multistate term-energy fit of ref. [3] to generate $T_{v,J \text{ parity}}$ energies for the low-lying $\Omega'' = \frac{1}{2}$ levels. The supermultiplet model of Gray *et al.* established that the low-lying $\Omega = \frac{1}{2}$ levels are almost 50:50 mixtures of the $^2\Sigma^+$ and $^2\Pi_{1/2}$ states of NiH. This is true for NiD, too, and although the expression for energy levels of a $^2\Sigma^+$ state (eq. 1) can be used to reproduce term energies of both states, it returns un-physical parameter values. As expected, though, the parity splittings at $J=0.5$ are opposite in sign for the two states: $E(v=0,f) - E(v=0,e) = 19.77 \text{ cm}^{-1}$ in $^2\Sigma^+$, and -9.07 cm^{-1} for $^2\Pi_{1/2}$.

$$\begin{aligned}
T_{v,F_1}(N) &= T_v + B_v N(N+1) - D_v [N(N+1)]^2 + \dots + \frac{1}{2}\gamma_1 N + \frac{1}{2}\gamma_2 N^2 + \dots \\
T_{v,F_2}(N) &= T_v + B_v N(N+1) - D_v [N(N+1)]^2 + \dots - \left(\frac{1}{2}\gamma_1 (N+1) + \frac{1}{2}\gamma_2 (N+1)^2 + \dots \right) \quad (1)
\end{aligned}$$

The information on the hitherto unobserved levels in NiD provide a stringent test on the predictions made by Abbasi *et al.* [3] from a multi-isotope fit of term energies to a modified version of the supermultiplet model originally proposed by Gray and Field[1]. Retaining spin-orbit interaction terms derived from a $\text{Ni}^+ 3d^9$ configuration, ref. [3] imposed simple mass-dependence of rotational and vibrational terms so that a single (though extensive) set of parameters could be used to represent vibronic energies of the spin-orbit coupled $^2\Sigma^+$, $^2\Pi$ and $^2\Delta$ states of $^{58,60,62}\text{NiH}$ and ^{58}NiD up to 6000 cm^{-1} above the electronic ground state. This non-standard model was not able to reproduce experimental precision for the observed term values, but was intended to guide future experimental work, indicating to within a few cm^{-1} where transitions should be expected. It served extremely well! The f parity term values determined for the $v=0$ level of the $^2\Sigma^+$ state from our spectra are within 1 cm^{-1} of predictions from the multi-isotope deperturbation fit, likewise for levels of e symmetry in the $v=0$ level of the $^2\Pi_{1/2}$ state (f parity overestimated by 6-8 cm^{-1}). The predictions placed $T_{J,e}$ and $T_{J+1,f}$ 7 cm^{-1} apart for $J=6.5$, $^2\Pi_{1/2} v=1$, initially making it hard to decide whether the weak features now labelled $P_f(J)$ in the lower part of Figure 2 were truly $P_f(J)$

lines, or $Q_{fe}(J+1)$. The assignments given in Table 1 were confirmed by re-recording fluorescence from the B $^2\Delta_{5/2}$ state $v=1$ with the 15% D₂ in argon mixture, and examining collisionally-induced fluorescence carefully.

Collisional energy transfer from the B $^2\Delta_{5/2}$ state $v=1$ populates another $\Omega'=1.5$ state, D[17.6] 1.5. Some of the weakest features in the spectrum could now be assigned as R_f lines in the (1-0) and (1-1) D[17.6] 1.5 \rightarrow $^2\Pi_{1/2}$ bands. Better still, the secure lower-state combination differences from the E[17.5]1.5 \rightarrow $^2\Sigma^+$ (1-0) spectra provided J and parity assignments for R_e, P_f, Q_{ef} and Q_{fe} branches from a 'new' excited $\Omega' = 1/2$ state with $T'_v \sim 16700$ cm⁻¹ (hereafter labelled [16.7]0.5), terminating on $v'' = 0$ of the low-lying $^2\Sigma^+$ state. These transitions are illustrated in Figure 4. The 'unassigned' feature mentioned in ref. [3] was the [16.7]0.5 - $^2\Sigma^+$ $v''=0$ R_e branch of this system (filled circles in Figure 4), easily spotted because it happens to fall between emission lines from stronger systems. The widely-spaced (~ 30 cm⁻¹) P_f transitions were nearly twice as strong, but less noticeable because they are interspersed with direct B-X₁ (1-2) fluorescence (the strongest lines of the P and Q branches of B-X₁ (1-2) go off the scale of Figure 4 by a factor ~ 8).

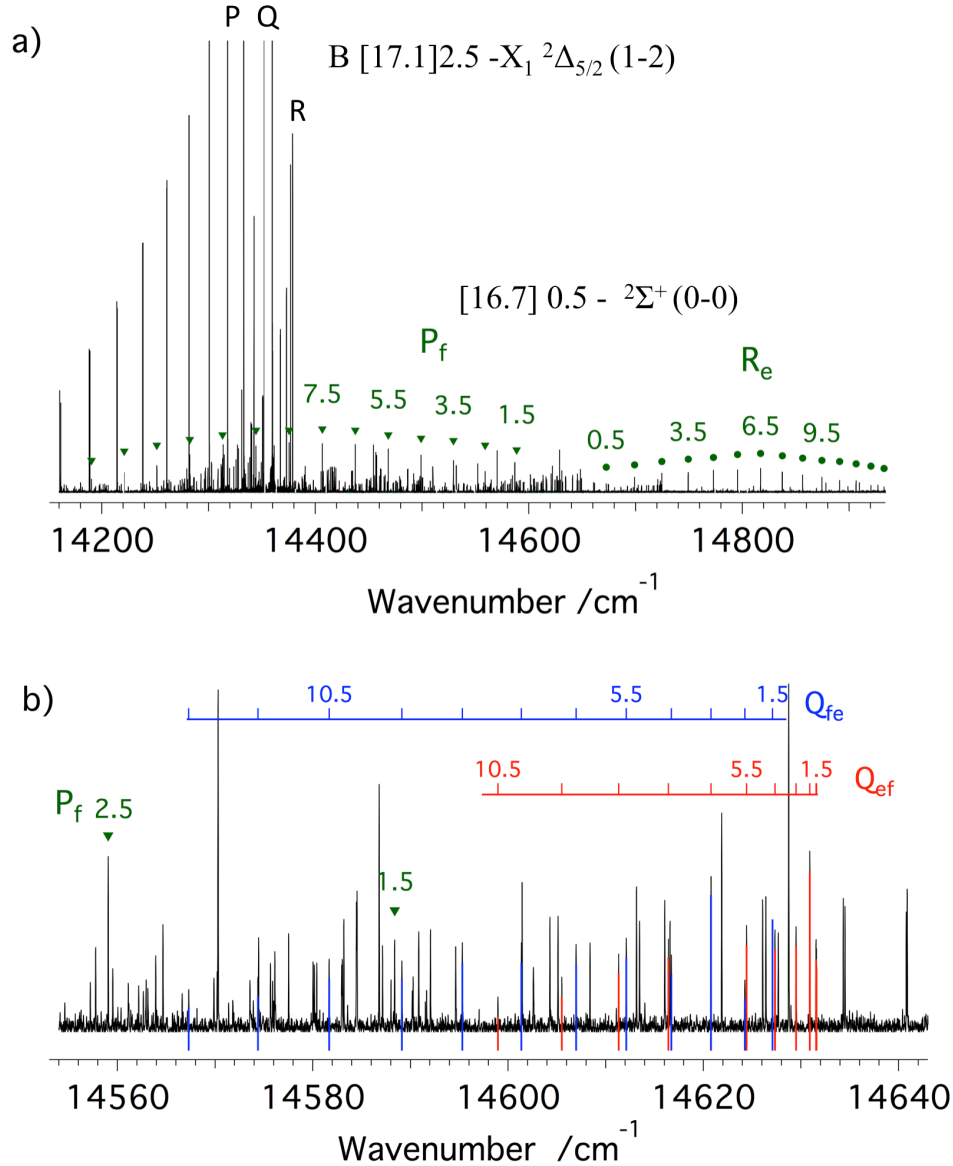


Figure 4 (in colour online). Collisionally-induced fluorescence in ^{58}NiD , following laser excitation of $^{58}\text{NiD } B^2\Delta_{5/2} v=1, J'_{e,f}=2.5$, showing transitions from the $[16.7]0.5$ upper state to the low-lying $^2\Sigma^+$ state, $v''=0$. Panel a) illustrates the distinctive, widely-spaced P_f (\blacktriangledown) and slightly weaker R_e (\bullet) branches). Panel b) highlights the crowded Q -branches between them; Q_{ef} with red line markers, Q_{fe} in blue, with markers extending below the experimental spectrum for clarity.

The lower portion of Figure 4 expands the Q -branch region between the P_f and R_e $[16.7]0.5 - ^2\Sigma^+ v''=0$ branches, where weak lines have now been assigned. Patterns are even less obvious, as these transitions appear together with emission from other collisionally-populated upper states: R lines of $I[17.4]1.5 - ^2\Pi_{3/2} (1-0)$, P lines of $E[17.5]1.5 - ^2\Pi_{3/2} (1-0)$, and R and Q lines of $B[16.0]2.5 - X_1^2\Delta_{5/2} (0-1)$ bands. Similar spectral patterns were assigned to R_e , P_f , Q_{ef} and Q_{fe} transitions to $^2\Sigma^+ v''=1$, but only P_f lines were seen to $^2\Sigma^+, v''=2$. Conversely, the R_f and

P_e branches were strong in emission to $v''=0$ of the W_2 ${}^2\Pi_{1/2}$ state. R_f lines are assigned with confidence (via an upper-state perturbation producing line – extra-line pairs) to $v''=1$, while the P_e assignments are based on some features barely emerging from noise that happen to match predictions for R_e transitions remarkably well; these are less secure. Given that Q branches appear in the $[16.7]0.5 \rightarrow {}^2\Sigma^+$ bands, and not in $[16.7]0.5 \rightarrow {}^2\Pi_{1/2}$, it seems reasonable to suggest that this new upper state has some ${}^2\Pi_{1/2}$ character. It is too low in energy to be the NiD analogue of the $[17.9]0.5$ state observed [5] in NiH. Figure 4 indicates an upper state vibrational assignment $v'=0$; this comes from the isotope shift $< 0.1 \text{ cm}^{-1}$ for the first rotational lines of the R and P branches in ${}^{58}\text{NiD}$ and ${}^{60}\text{NiD}$. The isotope splitting is expected to be $\sim 0.3 \text{ cm}^{-1}$ for $\Delta v = \pm 1$. The missing, or very weak, branches in the $[16.7]0.5 \rightarrow {}^2\Sigma^+$ and the $[16.7]0.5 \rightarrow {}^2\Pi$ bands are explained by destructive interference between parallel μ_{\parallel} and perpendicular μ_{\perp} transition moments to the spin-orbit-mixed lower states (${}^2\Pi_{1/2}$ and ${}^2\Sigma^+$ respectively). The strong branches are enhanced by constructive interference. These effects result from $\Delta\Lambda = \pm 1$ mixings produce opposing intensity changes for $\Delta J = +1$ and $\Delta J = -1$ lines, because transition amplitude phases are of opposite sign for the P and R lines of $\Delta\Lambda = \pm 1$ ‘perpendicular’ transitions [8]. The situation in NiD is illustrated schematically in Figure 5. Unexpectedly strong or weak P and R branches result from combinations of μ_{\perp} and μ_{\parallel} transition moments, for example,

$$\text{for } P(J) : \left[c_1\mu_{\parallel} - \sqrt{\frac{1}{2}}c_2\mu_{\perp} \right]^2 \text{ and for } R(J) : \left[c_1\mu_{\parallel} + \sqrt{\frac{1}{2}}c_2\mu_{\perp} \right]^2,$$

where signed eigenvector ‘parentage’ coefficients c_1 and c_2 multiply μ_{\perp} and μ_{\parallel} to determine the relative intensities of P(J) and R(J) lines. Similar patterns were seen in NiH from a higher-lying $\Omega' = 0.5$ state, and the phenomenon was discussed in some detail in ref. [5.] Figure 5 also shows that the parity splittings in the $[16.7]0.5$ state are even larger than in the lower ${}^2\Sigma^+$ state.

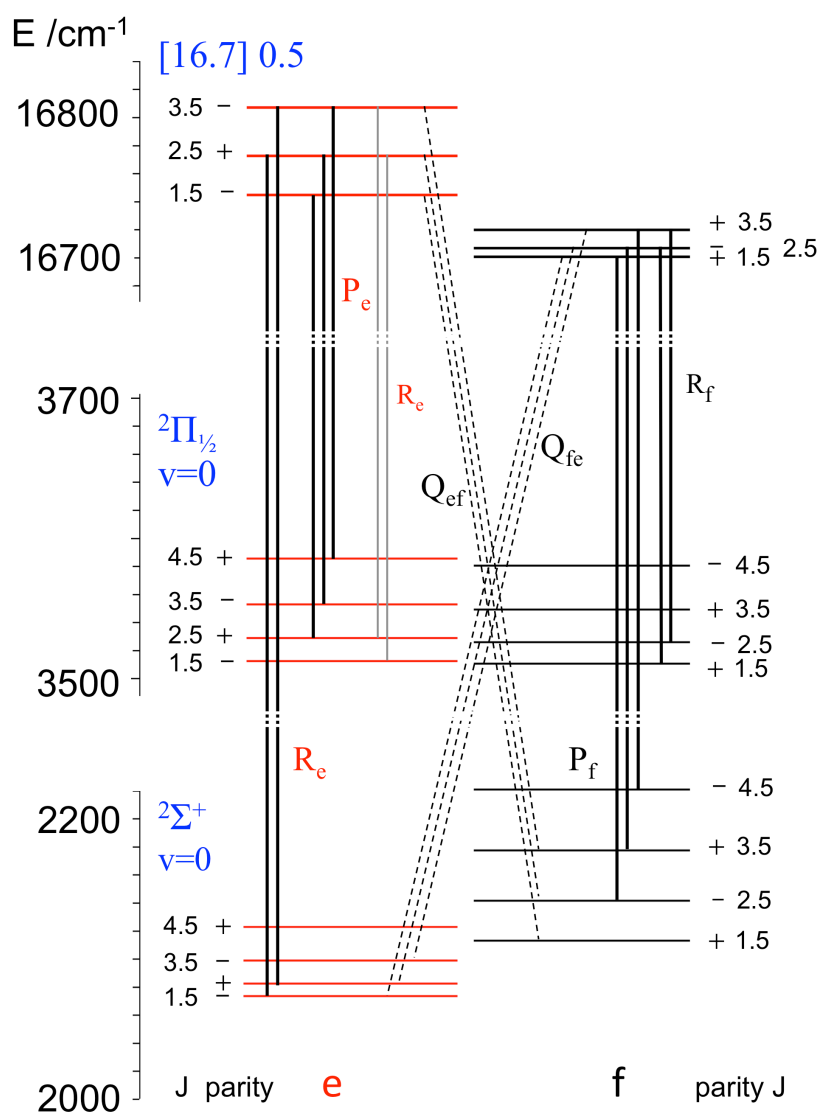


Figure 5 (in colour online). Heavy lines indicate the stronger branches (arising from constructive interference between transition dipole moments) observed in emission from the [16.7]0.5 excited state to $^2\Pi_{1/2}$ and $^2\Sigma^+$ lower states. The Q branches to $^2\Sigma^+$ are weaker (broken lines). Rotational stacks are drawn to scale within each state, indicating J and parity for e and f symmetry levels.

All assigned transitions from [16.7]0.5 (listed in table 2) were included in the multi-state term-value fit for ^{58}NiD , currently comprising ~ 2250 transitions and returning an unweighted root mean square deviation of 0.0056 cm^{-1} . Term energies for the $^2\Sigma^+$ state were reduced to effective band parameters (Table 3) using expression (1); the new data come from optical transitions shown schematically in Figure 6. A more restricted fit to eq (1) was used for [16.7]0.5 terms, eliminating

f-parity data with $J \geq 9.5$ (clearly affected by a local perturbation); the resulting parameters are shown in the last column of Table 3.

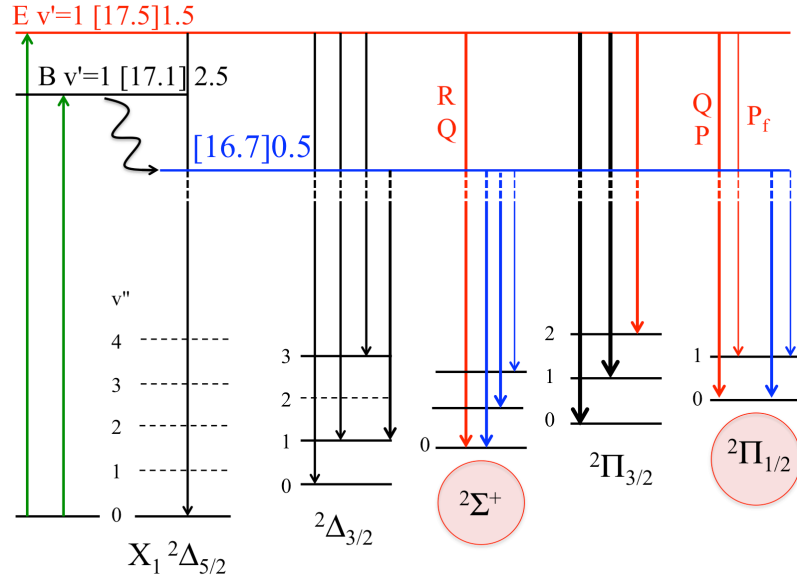


Figure 6 (in colour online). Schematic view of transitions defining previously unobserved levels of the low-lying supermultiplet states of ^{58}NiD . Upwards arrows indicate laser pump transitions, with the $\Omega'=0.5$ state populated by collisional energy transfer. Black downwards arrows connect to previously observed levels of the supermultiplet states. Thick lines denote strong bands.

Table 4 lists previously unreported term energies for levels of the 'supermultiplet states' of NiD extracted from the term-value fit. This includes not only levels of the $^2\Sigma^+$ and $^2\Pi_{1/2}$ states, but also $v=2$ of $^2\Pi_{3/2}$. Comparisons with predictions from Abbasi's work are also given. The agreement for the $\Omega'' = 0.5$ $v''=0$ levels of $^2\Sigma^+$ and $^2\Pi_{1/2}$ is remarkable. The predictions furthest from experiment were for $^2\Pi_{3/2}$ $v=2$, where the rotationless energy term was overestimated by 14 cm^{-1} .

The relative positions of the observed ligand-field state termvalues for NiH and NiD are illustrated in Figure 7. The plot emphasizes the modest difference in rotationless energies at $v=0$ for $^2\Pi_{1/2}$ and for $^2\Sigma^+$, contrasting with a very large shift between NiH and NiD for the $^2\Pi_{3/2}$ state. The proximity between $v \geq 1$ of the $^2\Delta_{3/2}$ state and $^2\Pi_{1/2}$ explains the abnormal parity splittings in the $^2\Delta_{3/2}$ state, noticed in [3] to be greater than in the $^2\Pi_{3/2}$ state.

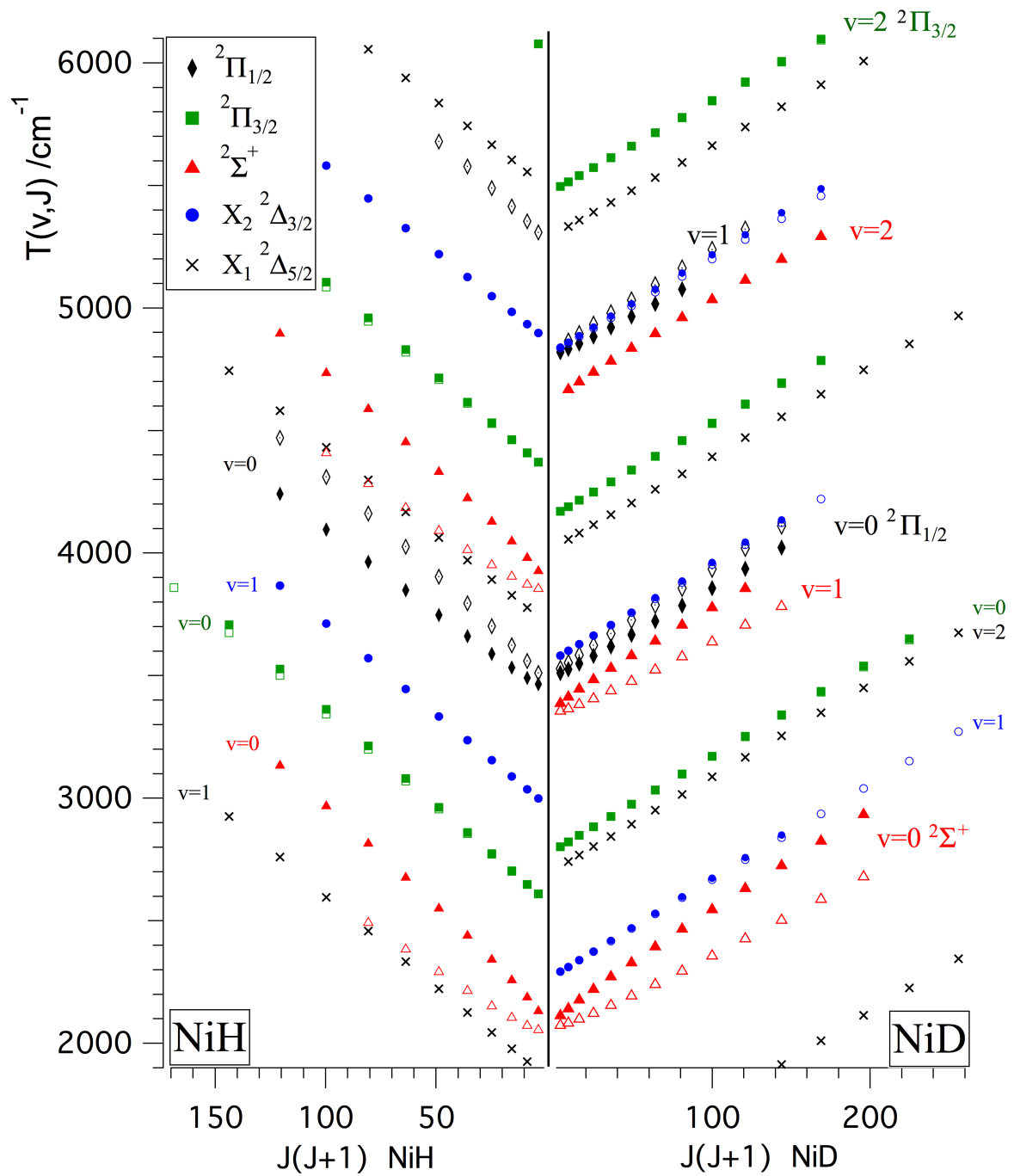


Figure 7 (in colour online) Term value plot for NiH and NiD in the region of the lowest vibrational levels of the ${}^2\Pi$ and ${}^2\Sigma^+$ states, large labels denoting new observations for ${}^2\Pi_{3/2}$ (squares), ${}^2\Pi_{1/2}$ (diamonds) and ${}^2\Sigma^+$ (triangles) in NiD. Open and filled symbols distinguish between e and f parity.

Conclusions

Finding the first rotational levels of the lowest $\Omega=1/2$ state ($v=0$ $^2\Sigma^+$) of NiD within 1 cm^{-1} of predictions is a triumph for Abbasi's multi-isotope Dunham parameter-based fit, with its various constraints and assumptions (off-diagonal spin-orbit, L- and S- uncoupling matrix elements derived from Ni^+ atomic properties, Born-Oppenheimer breakdown effects neglected, save for calculated mass-dependent zero-point energy shifts). Looking at the columns of differences between model predictions and current observations, the model overestimated the rotationless energy of $v=2$ in the $^2\Pi_{3/2}$ state, but reproduced the rotational structure quite well. On the contrary, the prediction for first rotational terms of $v=0$ and $v=1$ of the $^2\Pi_{1/2}$ state were remarkably good, within 2 cm^{-1} , but the parity splittings increase more quickly with J than the model predicted. At $J=7.5$ the energy term for e symmetry was underestimated by 5 cm^{-1} , with the f parity term overestimated by around 7 cm^{-1} . Additional information from spectra recorded after selective excitation of the lower abundance ^{60}NiD will, we hope, provide sufficient information to make a potential-curve fit option viable. There remain some unassigned features in the spectra not (yet) connected to known states of NiD, or even compatible with predictions, for which we cannot even offer tentative assignments. The remarks of A. Merer and co-workers' on spectra of CaF [9], " ... Rigorous assignment is frustrated only when multiple rotational transitions to a common upper state are unobservable because of systematic intensity effects", are highly pertinent in this case, too, as mixing between states causes 'allowed' branches to vanish in the electronic spectra of NiD.

Acknowledgements.

Financial support for this work came from NSERC Canada, and from CNRS France as an equipment grant from CSAA/INSU. AR thanks UNB for arranging a Harrison McCain visiting fellowship in 2017, and DT is grateful to support from the CNRS as chercheur invité, for 2 months spent at ILM in 2018.

References

- [1] J.A. Gray, M. Li, T. Nelis, and R.W. Field, *J. Chem. Phys.* **95**, 7164 (1991).
- [2] I. Havalyova, I. Bozhinova, A.J. Ross, P. Crozet, and A.E. Pashov, (2018). in *25th International Conference on High Resolution Molecular Spectroscopy, Bilbao (poster)* **P2-61** (2018).
- [3] M. Abbasi, A. Shayesteh, P. Crozet, and A.J. Ross, *J. Mol. Spectrosc.* **349**, 49 (2018).
- [4] C.T. Kingston, A.J. Merer, and T.D. Varberg, *J. Mol. Spectrosc.* **215** (1), 106 (2002).
- [5] A.J. Ross, P. Crozet, C. Richard, H. Harker, S.H. Ashworth, and D.W. Tokaryk, *Mol. Phys.* **110** (17), 2019 (2012).
- [6] J.-R. Guo, T.-T. Wang, Z.-X. Zhang, C.-X. Chen, and Y. Chen, *Chin. J. Chem. Phys.* **21**, 308 (2008).
- [7] R. Vallon, S.H. Ashworth, P. Crozet, R.W. Field, D. Forthomme, H. Harker, C. Richard, and A.J. Ross, *J. Phys. Chem. A* **113** (47), 13159 (2009).
- [8] H. Lefebvre-Brion and R.W. Field, *The spectra and dynamics of diatomic molecules* (Elsevier, Amsterdam, 2004), p. 387.
- [9] J.J. Kay, D.S. Byun, J.O. Clevenger, X. Jiang, V.S. Petrović, R. Seiler, J.R. Barchi, A.J. Merer, and R.W. Field, *Canadian Journal of Chemistry* **82** (6), 791 (2004).

Table 1

Compilation of assigned fluorescence transitions (cm^{-1}) from E[17.5] $\Omega = 1.5$. Estimated uncertainties 0.005 cm^{-1} for unblended lines.

E[17.5]1.5 \rightarrow ${}^2\Delta_{5/2} v''=0$						
J''	R_e	R_f	P_e	P_f	Q_{ef}	Q_{fe}
2.5			17508.136	17508.054		
3.5					17517.025	17516.245
4.5	17542.658				17508.802	17507.254
5.5					17487.101	17482.826
6.5					17473.655	17467.297
7.5					17458.488	17449.521
8.5					17441.619	17429.484
9.5						
E[17.5]1.5 \rightarrow ${}^2\Delta_{3/2} v''=0$						
J''	R_e	R_f	P_e	P_f	Q_{ef}	Q_{fe}
1.5	16549.705	16549.379			16534.390	16534.310
2.5	16551.227	16550.439	16514.426	16514.325		16529.425
3.5	16550.947	16549.370	16501.803	16501.432	16523.227	
4.5	16548.911	16546.125	16487.388	16486.513		
5.5	16545.129		16471.227	16469.501		
6.5		16532.970	16453.337	16450.364		
7.5			16433.751	16429.039		
8.5	16523.429		16412.482	16405.499		
9.5	16512.801	16496.081	16389.550	16379.718		
10.5	16500.482		16364.987	16351.702		
11.5	16486.499		16311.051	16321.451		
12.5			16281.694			
E[17.5]1.5 \rightarrow ${}^2\Delta_{3/2} v''=2$						
J''	R_e	R_f	P_e	P_f	Q_{ef}	Q_{fe}
1.5	13941.461	13941.084				
2.5	13943.467	13942.457	13906.666	13906.345		
3.5	13943.913	13941.791	13894.759	13893.871		
4.5	13942.837	13939.010	13881.309	13879.400		
5.5	13940.254	13934.009	13866.353	13862.839		
6.5	13936.174	13926.740	13849.895	13844.128		
7.5	13930.609	13917.130	13831.973	13823.200		
8.5	13923.505	13905.176	13812.562	13799.997		
9.5	13914.344	13890.893				
10.5	13904.813	13874.344	13768.862			
11.5	13891.856	13855.344				
E[17.5]1.5 \rightarrow ${}^2\Delta_{3/2} v''=3$						
J''	R_e	R_f	P_e	P_f	Q_{ef}	Q_{fe}
1.5		12682.551				
2.5	12688.238	12683.888	12651.444	12647.779		
3.5	12689.044	12683.257	12639.891	12635.329		
4.5	12688.699	12680.595	12627.166	12620.980		
5.5	12687.086	12675.839	12613.180	12604.665		
6.5		12668.924	12597.925	12586.314		

7.5	12680.053		12581.426	12565.893		
8.5	12674.670		12563.709	12543.362		
9.5	12668.059	12635.119	12544.820			
10.5	12660.247	12619.608	12524.758			
11.5	12651.246		12503.568	12463.290		
12.5			12481.264	12432.625		
E[17.5]1.5 \rightarrow $^2\Pi_{3/2} v''=0$						
J''	R_e	R_f	P_e	P_f	Q_{ef}	Q_{fe}
1.5	14720.820	14720.497			14705.499	14705.426
2.5	14723.037	14722.234	14686.251	14686.131	14701.527	14701.248
3.5	14723.777	14722.142	14674.625	14674.216	14696.016	14695.339
4.5	14723.037	14720.153	14661.503	14660.539	14688.984	
5.5	14720.820	14716.213	14646.917	14645.045	14680.442	14678.098
6.5	14717.170	14710.283	14630.897	14627.679	14670.419	14666.669
7.5	14712.090	14702.325	14613.465	14608.392		
8.5	14705.596	14692.337	14594.644	14587.152		
9.5	14697.694	14680.315	14574.456	14563.926		
10.5	14688.400	14666.297	14552.915	14538.712		
11.5	14677.732	14650.324	14530.056	14511.528		
12.5	14666.289	14632.483	14505.883	14482.408		
13.5			14480.407	14451.411		
14.5			14453.656	14418.612		
E[17.5]1.5 \rightarrow $^2\Pi_{3/2} v''=1$						
J''	R_e	R_f	P_e	P_f	Q_{ef}	Q_{fe}
1.5		13352.422			13337.418	13337.346
2.5	13355.476	13354.663			13333.949	13333.672
3.5	13356.913	13355.276	13307.761	13307.351	13329.144	13328.460
4.5	13357.072	13354.197	13295.537	13294.581	13323.030	13321.662
5.5	13355.973	13351.375	13282.068	13280.197	13315.608	
6.5	13353.641	13346.765	13267.360	13264.160		
7.5	13350.086	13340.338	13251.454	13246.402		
8.5	13345.324	13332.082	13234.369	13226.896		
9.5	13339.377	13322.004	13216.132	13205.617		
10.5	13332.263	13310.144	13196.767	13182.562		
11.5	13323.982	13296.545	13176.299	13157.744		
12.5	13314.563					
E[17.5]1.5 \rightarrow $^2\Pi_{3/2} v''=2$						
J''	R_e	R_f	P_e	P_f	Q_{ef}	Q_{fe}
1.5		12026.553			12011.555	12011.483
2.5	12030.108		11993.312	11993.185		12008.310
3.5	12032.253			11982.666	12004.466	
4.5	12033.323	12030.407	11971.791			
5.5	12033.356	12028.668	11959.450			
6.5		12025.338	11946.088	11942.729		
7.5	12030.377		11931.749	11926.457		
8.5	12027.417			11908.626		
9.5	12023.514	12005.611	11900.272			
10.5	12018.685	11995.834	11883.198			
11.5	12012.971		11865.291	11845.713		
12.5			11846.581	11821.663		
13.5			11827.114			

E[17.5]1.5 \rightarrow $^2\Sigma^+$ $v''=0$						
J''	R_e	R_f	P_e	P_f	Q_{ef}	Q_{fe}
0.5	15435.755	15415.898				
1.5	15449.693	15409.878			15394.877	15434.297
2.5	15462.259	15402.366			15381.652	15440.458
3.5	15473.456	15393.343			15367.220	15445.016
4.5	15483.285	15382.776			15351.608	15447.887
5.5	15491.733	15370.656			15334.886	15449.000
6.5	15498.787	15356.972	15412.515		15317.098	15448.287
7.5	15504.446	15341.724	15405.825		15298.281	15445.689
8.5	15508.692	15324.912			15278.495	15441.167
9.5	15511.519	15306.614			15257.757	15434.690
10.5	15512.908	15286.846			15236.091	15426.266
11.5	15512.829				15213.521	15415.914
12.5			15351.502		15190.024	15403.665
13.5			15336.421			15389.575
E[17.5]1.5 \rightarrow $^2\Pi_{1/2}$ $v''=0$						
J''	R_e	R_f	P_e	P_f	Q_{ef}	Q_{fe}
0.5	13995.445	14004.428				
1.5	13994.463	14012.235			13997.222	13979.069
2.5	13991.893		13955.103	13981.907	13997.309	13970.104
3.5			13938.614	13973.771	13995.565	13959.326
4.5			13920.596	13963.545	13991.986	13946.725
5.5			13901.105		13986.532	13932.282
6.5			13880.193	13936.479	13979.205	13915.962
7.5			13857.909	13919.529		13897.784
8.5			13834.335	13900.321	13959.070	
9.5			13809.608	13878.903		
10.5			13783.896	13855.373		13832.758
11.5			13757.526	13829.866		13808.287
E[17.5]1.5 \rightarrow $^2\Pi_{1/2}$ $v''=1$						
J''	R_e	R_f	P_e	P_f	Q_{ef}	Q_{fe}
6.5				12638.174		
7.5				12624.959		
8.5				12609.982		

Table 2

Compilation of assigned fluorescence transitions (cm^{-1}) from [16.7] $\Omega' = 0.5$ to lower states ${}^2\Delta_{3/2}$, ${}^2\Sigma^+$ and ${}^2\Pi_{1/2}$. Estimated uncertainties 0.005 cm^{-1} for unblended lines, 0.015 cm^{-1} for particularly weak branches(#). Asterisks indicate extra-lines with $J'=9.5$, f.

[16.7]0.5 \rightarrow ${}^2\Delta_{3/2}$ $v''=0$						
J''	R_e	R_f	P_e	P_f	Q_{ef}	Q_{fe}
1.5						
2.5					overlap /	15713.221
3.5					HeNe	15698.278
4.5						15682.353
5.5						15665.503
6.5						15647.794
7.5						15629.288
8.5						15610.056
9.5						15590.405
9.5						*15589.297
10.5						15569.255
11.5						15548.050
[16.7]0.5 \rightarrow ${}^2\Delta_{3/2}$ $v''=1$						
J''	R_e	R_f	P_e	P_f	Q_{ef}	Q_{fe}
1.5			14431.445	14409.409		14408.594
2.5	14495.243	14407.819	14432.880	14388.729	14460.583	14394.953
3.5	14508.783	14399.992	14433.162	14367.013	14467.298	14380.386
4.5	14521.057	14391.201	14432.270	14344.264	14472.642	14364.958
5.5	14532.062	14381.484	14431.445	14320.449	14476.564	14348.743
6.5	14541.763	14370.866			14479.020	14331.817
7.5					14479.940	14314.235
8.5		14347.332			14479.295	14296.086
8.5		*14346.209				
9.5		14333.570			14477.053	14277.676
9.5						*14276.569
10.5					14473.179	14257.926
11.5					14467.638	14238.262
12.5					14460.425	
13.5					14451.509	
[16.7]0.5 \rightarrow ${}^2\Sigma^+$ $v''=0$						
J''	R_e	R_f	P_e	P_f	Q_{ef}	Q_{fe}
0.5	14672.463				14631.533	
1.5	14698.942			14588.383	14631.586	14627.076
2.5	14724.531			14559.053	14630.901	14624.247
3.5	14749.177			14529.207	14629.488	14620.783
4.5	14772.824			14498.933	14627.326	14616.724
5.5	14795.421			14468.323	14624.423	14612.107
6.5	14816.919			14437.471	14620.783	14606.970
7.5	14837.277			14406.471	14616.419	14601.361
8.5	14856.446			14375.408		14595.318
9.5	14874.386			14344.380		14589.124
9.5						*14588.013
10.5	14891.051			14313.697		
10.5				*14312.588		
11.5	14906.395			14282.286		
12.5	14920.340					
13.5	14932.688					

[16.7]0.5 \rightarrow $^2\Sigma^+$ $v''=1$

J''	R_e	R_f	P_e	P_f	Q_{ef}	Q_{fe}
0.5	13391.926				13354.543	
1.5	13417.217			13313.863	13357.069	
2.5	13441.962			13287.534	13359.393	13341.679
3.5	13466.071			13261.286	13361.572	13337.681
4.5	13489.461			13235.269	13363.666	13333.360
5.5	13512.059			13209.619	13365.717	13328.744
6.5	13533.795			13184.446	13367.758	13323.849
7.5	13554.608			13159.825	13369.778	13318.691
8.5	13574.447			13135.782	13371.701	13313.317
9.5	13593.247			13112.304	13373.429	13307.981
9.5						*13306.874
10.5	13610.961			13089.571		13301.584
10.5				*13088.461		
11.5	13627.521					13295.529

[16.7]0.5 \rightarrow $^2\Sigma^+$ $v''=2$

J''	R_e	R_f	P_e	P_f	Q_{ef}	Q_{fe}
1.5						
2.5				12034.035		
3.5				12007.947		
4.5				11981.962		
5.5				11956.172		
6.5				11930.653		
7.5				11905.472		
8.5				11880.676		
9.5				11856.317		
10.5				11832.664		
10.5				*11831.554		
11.5				11808.587		
12.5				11785.479		

[16.7]0.5 \rightarrow $^2\Pi_{1/2}$ $v''=0$

J''	R_e	R_f	P_e	P_f	Q_{ef}	Q_{fe}
0.5		13197.228				
1.5	13243.724	13196.017	13194.714			
2.5	13254.173	13193.783	13191.831			
3.5	13263.487	13190.539	13187.867			
4.5	13271.662	13186.265	13182.875			
5.5	13278.701	13180.991	13176.824			
6.5	13284.595	13174.747	13169.727			
7.5	13289.343	13167.612	13161.600			
8.5	13293.053	13159.927	13152.472			
8.5		*13158.817				
9.5	13295.723	13150.688	13142.423			
10.5	13297.540	13141.422	13131.639			
11.5	13298.760		13120.405			

[16.7]0.5 \rightarrow ${}^2\Pi_{1/2} v''=1$

J''	R_e	R_f	P_e	P_f	Q_{ef}	Q_{fe}
0.5		11887.700				
1.5		11887.158				
2.5		11886.025	11880.951			
3.5		11884.338	11878.061			
4.5	11962.889	11882.152	11874.083			
5.5	11971.013	11879.504	11869.130			
6.5	11978.120	11876.443	11863.235			
7.5	11984.188	11873.041	11856.426			
8.5		11869.593	11848.641			
8.5		*11868.491				
9.5	11993.190		11839.910			
10.5			11830.183			

Table 3.

Effective parameters for vibrational levels $v = 0-2$ of the low-lying $^2\Sigma^+$ state of ^{58}NiD , fitting term values to eq. 1. Although these fitting parameters (quoted with 1 standard deviation in units of last digit in parenthesis) have little physical meaning, they reproduce the term energies with 0.014 cm^{-1} unweighted root mean square deviation. The last column gives parameters fitting term values $J \leq 12.5$ e and $J \leq 8.5$ f of the hitherto unobserved [16.7] 0.5 upper state to eq. 1. This fit returns an unweighted rms deviation of 0.02 cm^{-1} .

Parameter (cm^{-1})	$^2\Sigma^+, v=0$	$^2\Sigma^+, v=1$	$^2\Sigma^+, v=2$	[16.7] 0.5
T_v	2073.333 (6)	3353.833 (8)	4606.791(23)	16724.53(1)
B_v	3.75575(36)	3.55749 (66)	3.4067 (10)	3.3800(3)
D_v	$2.0486(52) \times 10^{-4}$	$4.713(131) \times 10^{-4}$	$1.7288(1280) \times 10^{-4}$	$1.73(33) \times 10^{-5}$
H_v	$1.612(195) \times 10^{-7}$	$1.429 (73) \times 10^{-6}$	$3.153(440) \times 10^{-7}$	
γ_{v1}	-12.289(3)	-9.182 (3)	-10.0	28.828(4)
γ_{v2}	$8.372(56) \times 10^{-3}$	$2.534 (12) \times 10^{-2}$		-0.01468(4)
γ_{v3}	$-2.33(26) \times 10^{-6}$	$-3.543(87) \times 10^{-5}$		

Table 4

Comparison of experimentally determined term energies for levels of $^2\Sigma^+$ ($v=0$), $^2\Pi_{1/2}$ ($v=0,1$) and $^2\Pi_{3/2}$ ($v=2$) with predictions from the multi-isotope fit of ref. [3].

J	e/f	$^2\Sigma^+$ $v=0$		$^2\Sigma^+$ $v=1$		$^2\Sigma^+$ $v=2$	
		T_{vJ} (Exp) (cm^{-1})	Exp-Pred (cm^{-1})	T_{vJ} (Exp) (cm^{-1})	Exp-Pred (cm^{-1})	T_{vJ} (Exp) (cm^{-1})	Exp-Pred (cm^{-1})
0.5	e	2072.396	0.1	3352.937	1.6		
0.5	f	2092.166	0.0	3369.166	2.6		
1.5	e	2073.768	0.3	3355.496	1.2		
1.5	f	2113.273	-0.1	3387.793	3.1		
2.5	e	2082.691	0.4	3365.260	0.8		
2.5	f	2141.808	-0.1	3413.322	3.8	4666.823	7.4
3.5	e	2099.158	0.6	3382.260	0.4		
3.5	f	2177.730	-0.1	3445.651	4.4	4698.992	7.9
4.5	e	2123.190	0.8	3406.551	0.1		
4.5	f	2221.010	0.0	3484.668	5.1	4737.978	8.5
5.5	e	2154.788	1.1	3438.147	-0.2		
5.5	f	2271.592	0.1	3530.294	5.9	4783.740	9.2
6.5	e	2193.963	1.4	3477.085	-0.5		
6.5	f	2329.423	0.1	3582.447	6.7	4836.238	9.9
7.5	e	2240.703	1.7	3523.369	-0.8		
7.5	f	2394.464	0.2	3641.105	7.2	4895.462	10.6
8.5	e	2295.013	2.0	3577.009	-1.0		
8.5	f	2466.658	0.4	3706.277	7.8	4961.384	11.3
9.5	e	2356.880	2.4	3638.021	-1.3		
9.5	f	2545.945	0.5	3778.025	8.4	5034.012	12.1
10.5	e	2426.290	2.8	3706.384	-1.5		
10.5	f	2632.308	0.7			5113.340	12.9
11.5	e	2503.245	3.2	3782.102	-1.7		
11.5	f	2725.676	0.8			5199.381	13.6
12.5	e	2587.695	3.7				
12.5	f	2826.053	1.0			5292.146	14.4
13.5	e	2679.656	4.2				

J	e/f	$^2\Pi_{1/2}$ $v=0$		$^2\Pi_{1/2}$ $v=1$		$^2\Pi_{3/2}$ $v=2$	
		T_{vJ} (Exp) (cm^{-1})	Exp-Pred (cm^{-1})	T_{vJ} (Exp) (cm^{-1})	Exp-Pred (cm^{-1})	T_{vJ} (Exp) (cm^{-1})	Exp-Pred (cm^{-1})
0.5	e	3512.706	1.4				
0.5	f	3503.636	-0.1	4813.158	-3.8		
1.5	e	3528.997	2.0			5496.580	-14.1
1.5	f	3510.922	-0.9	4819.783	-4.1	5496.596	-14.1
2.5	e	3553.050	2.6	4863.896	-1.2	5514.837	-14.1
2.5	f	3526.156	-1.8	4833.913	-4.5	5514.878	-14.1
3.5	e	3584.847	3.1	4894.562	-1.4	5540.362	-14.2
3.5	f	3549.382	-2.8	4855.571	-4.9	5540.481	-14.1
4.5	e	3624.351	3.6	4933.131	-1.2	5573.154	-14.2
4.5	f	3580.630	-3.9	4884.743	-5.4	5573.379	-14.1

5.5 e	3671.507	4.1	4979.197	-1.0	5613.164	-14.2
5.5 f	3619.944	-5.1	4921.430	-5.9	5613.580	-14.1
6.5 e	3726.285	4.6	5032.768	-0.8	5660.388	-14.2
6.5 f	3667.314	-6.3	4965.615	-6.3	5661.056	-14.1
7.5 e	3788.612	5.0	5093.784	-0.6	5714.772	-14.2
7.5 f	3722.718	-7.3	5017.289	-6.8	5715.789	-14.0
8.5 e	3858.417	5.4	5162.239	-0.4	5776.285	-14.3
8.5 f*	3786.077	-7.7	5076.408	-7.3	5777.766	-14.0
9.5 e	3935.543	5.7	5238.075	-0.2	5844.879	-14.3
9.5 f*	3857.282	-8.1			5846.945	-13.9
10.5 e	4019.804	5.7	5321.270	0.0	5920.507	-14.4
10.5 f*	3936.199	-8.3			5923.321	-13.8
11.5 e	4110.870	5.4			6003.105	-14.5
11.5 f*	4022.692	-8.5			6006.843	-13.7
